Measurement and modeling of damping for time-domain structural acoustics simulations

Benjamin Cotté, Augustin Parret-Fréaud, Antoine Chaigne

Denver, Colorado
NOISE-CON 2013
2013 August 26-28

Measurement and Modeling of Damping for Time-Domain Structral Acoustics Simulations

Benjamin Cotté
Augustin Parret-Fréaud
Antoine Chaigne
Department of Mechanical Engineering (UME)
ENSTA ParisTech
828, boulevard des Maréchaux
91762 Palaiseau Cedex FRANCE
benjamin.cotte@ensta-paristech.fr

ABSTRACT

This work deals with the measurement and time-domain modeling of damping in structural acoustics. An experimental technique based on the plate impulse response measurement is presented to estimate the damping factor over a wide frequency band. This technique is succesfully applied to a nylon plate between 100 Hz and 15 kHz approximately. Then we present an original approach that consists in representing the measured frequency variations of damping by a digital filter that meets the criteria of causality and stability, and then in transposing it into the time domain. Time-domain simulations of the longitudinal vibrations of a nylon bar are performed to show the efficiency of our approach, where the filter parameters are estimated from the experimental data through an optimization procedure.

1 INTRODUCTION

Acoustic radiation of impacted structure strongly depends on its damping properties, and more specifically on the frequency dependence of damping. This study aims at measuring damping over a wide frequency range, and to model the vibroacoustic behavior of structures in the time domain. We focus mainly on the behavior of viscoelastic materials (polymers, composites, wood) that can be found in different applications such as transportation noise, building acoustics and musical acoustics.

First, an experimental technique aiming at estimating the damping factor over a wide frequency range is presented and applied to a nylon plate in Section 2. This technique is based on a time-frequency analysis of the plate impulse response and on the use of energy decay relief. Second, we present in Section 3 a time-domain model that uses digital filters to accurately represent the material constitutive law. Conditions are derived to guarantee that this model is causal, stable and dissipative. Finally, time-domain simulations of the longitudinal vibrations of a nylon bar are performed in Section 4 to show the efficiency of our approach.

2 DAMPING ESTIMATES FROM PLATE IMPULSE RESPONSE MEASUREMENTS

A. Plate impulse response measurement

To obtain good estimates of the damping factor, the plate impulse response (IR) needs to be measured with a high signal to noise ratio (at least 30 dB). That is why we choose to use the method proposed by Farina [1] to measure room IR, that has also been applied to a reverberant plate by Arcas and Chaigne [2].

The IR $h(t)$ between an excitation signal $x_e(t)$ and a vibration signal $y(t)$ is defined as $y(t) = h(t) \otimes x_e(t)$, where $\otimes$ is the convolution product. Using a deterministic signal $x_e(t)$ whose inverse filter f_i is known enables us to obtain the impulse response through $h(t) = y(t) \otimes f_i(t)$. Moreover, Farina suggests to use a logarithmic sweep excitation:

$$x_e(t) = \sin\left[\frac{\omega_1 T}{\ln(\omega_2/\omega_1)}\left(e^{\frac{t}{T}\ln(\omega_2/\omega_1)-1}\right)\right], \tag{1}$$

where ω_1 and ω_2 are the minimum and maximum angular frequencies of the excitation, and T_s is the signal duration. Using a logarithmic sweep is particularly interesting since it allows us to separate the linear and nonlinear parts of the IR to keep only the linear part in the following.

Farina's method is applied on a nylon (PA6) plate of dimensions 52 cm×30 cm and of thickness 6 mm. The plate is excited by a Bruel&Kjaer 4810 shaker at the center of the plate and the vibration is measured close to the edge by a Bruel&Kjaer 4394 accelerometer. Three measurements on overlapping frequency bands are performed ; the characteristics of the corresponding excitation signals are given in Table 1. The impulse response for measurement N1 between 20 Hz and 1200 Hz is plotted in Figure 1(a).

Table 1: Characteristics of the excitation signals for nylon plate measurements: $[f_1, f_2]$ is the frequency band of interest, T_s is the sweep duration and F_s the sampling frequency.

Measurement	$[f_1, f_2]$ (Hz)	T_s (s)	F_s (kHz)
N1	[20,1200]	60	22.05
N2	[1000,5000]	60	22.05
N3	[4000,16 000]	60	44.15

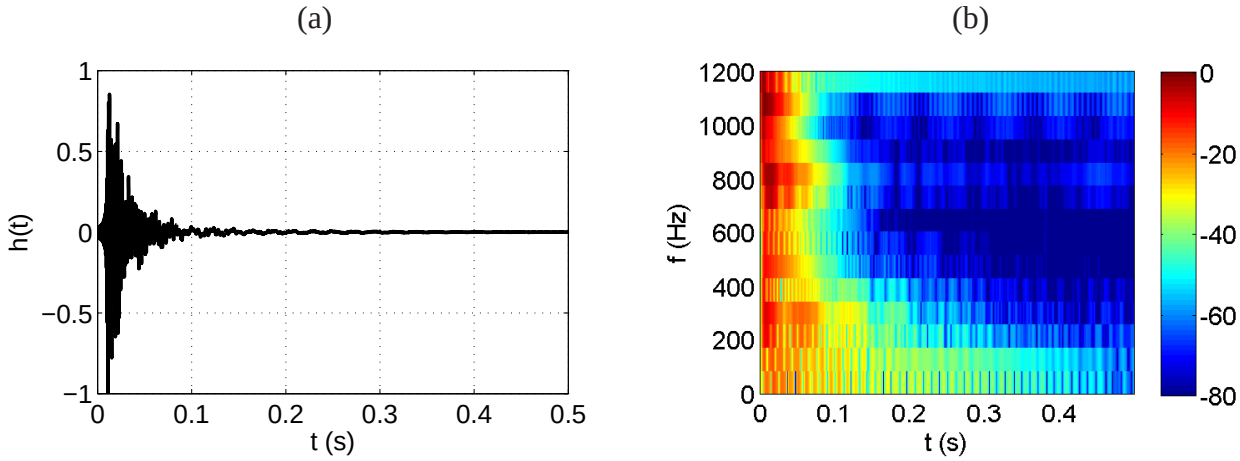

Figure 1: (a) Impulse response of measurement N1 and (b) associated spectrogram with $\Delta f = 86$ Hz and $\Delta t = 1.2$ ms.

B. Calculation of energy decay relief

A time-frequency analysis is performed on the impulse response in order to calculate the Energy Decay Relief (EDR), that is a spectral development of the integrated Energy Decay Curve introduced by Schroeder. Let $H_{m,k} = H(m\Delta t, k\Delta f)$ be the short-time Fourier transform or spectrogram of the IR $h(t)$, then the EDR at time $t_n = n\Delta t$ on the frequency bin $f_k = k\Delta f$ is defined as:

$$EDR(t_n, f_k) = \sum_{m=n}^{M} |H_{m,k}|^2. \tag{2}$$

$EDR(t_n, f_k)$ is the total amount of energy at frequency f_k that remains in the IR after a given time t_n. The upper limit M of the sum in Equation (2) corresponds to the time $t_M = M\Delta t$ after which the IR is contaminated by noise. From a practical point of view, it is taken as the mean measured noise level plus 8 dB.

The spectrogram is calculated using a Hanning window, an overlap rate r and N_{FFT} points in the Fast Fourier Transform calculation. The associated frequency and time resolutions are $\Delta f = F_s/N_{FFT}$ and $\Delta t = N_{FFT}(1-r)/F_s$. The spectrogram of measurement N1 is plotted in Figure 1(b) using $N_{FFT} = 256$ and $r = 90\%$, which yields $\Delta f = 86$ Hz and $\Delta t = 1.2$ ms. The EDR of measurement N3 on the frequency bands $f_k = 5509\,Hz$ and $f_k = 13\,797\,Hz$ are plotted in Figure 2. These curves are monotonously decreasing and the damping factor will be estimated from the slope of the linear part of these curves.

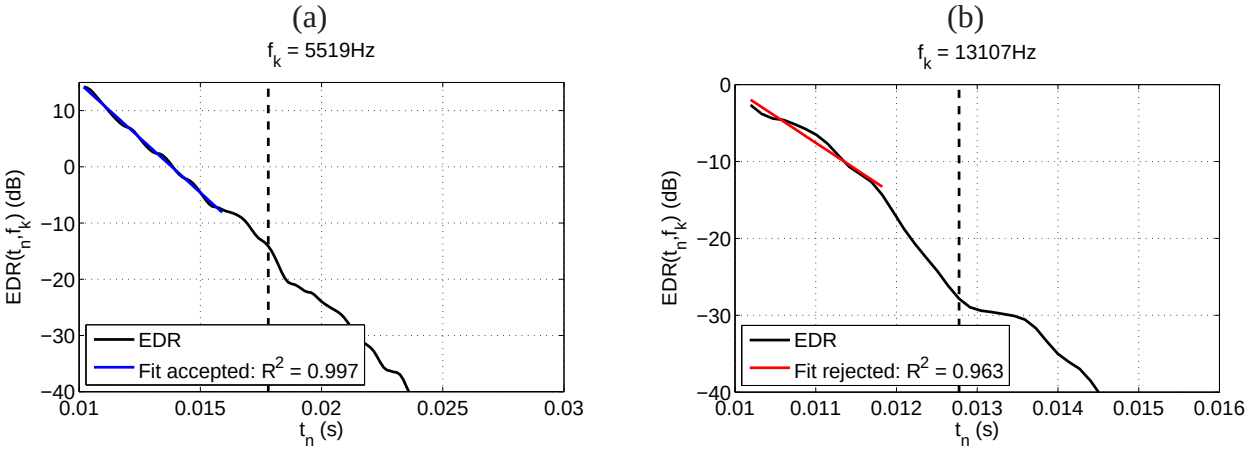

Figure 2: Energy decay reliefs $EDR(t_n, f_k)$ for frequency bands centered at (a) 5509 Hz, and (b) 13 797 Hz obtained from measurement N3 with a frequency resolution of 690 Hz and a time resolution of 0.14 ms. The dashed vertical lines correspond to time $t_M/2$.

C. Frequency dependence of damping from energy decay reliefs

The damping factor $\alpha(f_k)$ is given by:

$$\alpha(f_k) = -K_{dB}(f_K)\ln 10/20, \tag{3}$$

where $K_{dB}(f_K)$ is the linear part of the EDR slope at frequency f_k (in dB/s) that is obtained by fitting its N_s first time samples. Since it is not obvious to know N_s *a priori*, N_s is increased from N_{s1} to N_{s2}, where N_{s1} is the sample corresponding to a 10 dB decrease of the EDR, and $N_{s2} = M/2$. Thus $(N_{s2} - N_{s1} + 1)$ estimates are obtained with their associated linear correlation coefficient R^2. The estimate with the largest linear correlation coefficient is finally kept, except if R^2 is lower than a threshold value that we arbitrarily set at 99%. In Figure 2, the fit at $f_k = 5519$ Hz is accepted ($R^2 = 99.7\%$), however the fit at $f_k = 13\,107$ Hz is rejected ($R^2 = 96.3\%$) and we observe that the EDR at this frequency does not show a clear linear decrease.

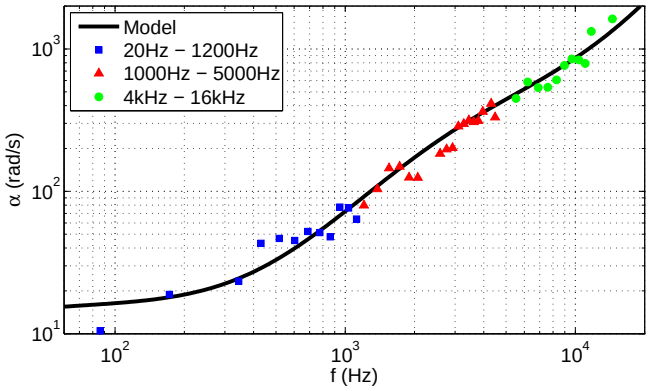

Figure 3: Frequency dependence of the damping factor α for measurements N1, N2 and N3 (symbols) and for Collet *et al.* [3] model (solid line).

The damping factor is estimated using different frequency and time resolution for measurements N1, N2 and N3: $\Delta f = 86Hz$ and $\Delta t = 1.2$ ms for N1, $\Delta f = 172Hz$ and $\Delta t = 0.59$ ms for N2, $\Delta f = 690Hz$ and $\Delta t = 0.14$ ms for N3. A better time resolution is needed at high frequency because damping is higher and the EDR decreases very fast at these frequencies. The damping factor is plotted with respect to frequency in Figure 3. A total of 40 frequency estimates are displayed between 86 Hz and 14487 Hz showing the increase of α from 10 rad/s to more than 1000 rad/s. A model proposed by Collet *et al.* [3] for nylon is also plotted in Figure 3 and is in good agreement with our measurements.

3 TIME-DOMAIN SIMULATIONS OF DAMPED STRUCTURES USING DIGITAL FILTERS

A. Problem studied

We consider the one-dimensional problem of the longitudinal vibrations of a cantilever beam of length L and density ρ. Let $u(x,t)$, $\varepsilon(x,t)$ and $\sigma(x,t)$ be the displacement, strain and stress of the beam. The equations of the problem in the small perturbation approximation are:

$$\sigma(x,t) = \mathscr{E}(\varepsilon(x,t)) = \mathscr{E}\left(\frac{\partial u(x,t)}{\partial x}\right), \tag{4a}$$

$$\rho \frac{\partial^2 u(x,t)}{\partial t^2} = \frac{\partial \sigma(x,t)}{\partial x} + f(x,t), \tag{4b}$$

with $\mathscr{E}$ the material constitutive law that is assumed to be linear, $f(x,t)$ an external force distribution, and with boundary conditions $u(0,t) = 0$ and $\sigma(L,t) = 0$.

B. Modeling the material law using a digital filter

Up to now, no material constitutive law $\mathscr{E}$ has been chosen. Instead of discretizing a continous time-domain model, we decide to represent it directly in discrete time by a digital filter. We introduce the time step Δt (sampling rate $F_s = 1/\Delta t$), and we note $\sigma^n(x) = \sigma(x,t^n)$ and $\varepsilon^n(x) = \varepsilon(x,t^n)$ the values of σ and ε at time $t^n = n\Delta t$. Generally speaking, any linear time-invariant digital filter can be defined as:

$$\sigma^{n+1}(x) = H_0\left(\varepsilon^{n+1}(x) + \sum_{l=1}^{N_b} b_l \varepsilon^{n+1-l}(x)\right) - \sum_{m=1}^{N_a} a_m \sigma^{n+1-m}(x). \tag{5}$$

The properties of such filter are classically studied from its transfer function $H(z)$ in the frequency domain using the Z-transform:

$$H(z) = H_0 \left[\frac{1 + \sum_{l=1}^{N_b} b_l z^{-l}}{1 + \sum_{m=1}^{N_a} a_m z^{-m}} \right] = H_0 \left[\frac{\prod_{l=1}^{N_b} \left(1 - q_l z^{-l}\right)}{\prod_{m=1}^{N_a} \left(1 - p_m z^{-l}\right)} \right], \tag{6}$$

where $(p_m)_{1 \leq m \leq N_a}$ are the poles, and $(q_l)_{1 \leq l \leq N_b}$ are the zeros of the filter. To guarantee the causality and stability of the filter, the poles must verify [4]:

$$|p_m| \leq 1, \ \forall 1 \leq m \leq N_a. \tag{7}$$

In the following, we will consider a constitutive law made of a series of N_f first order filters ($N_a = N_b = 1$) in parallel:

$$\sigma^{n+1}(x) = \sum_{k=1}^{N_f} \sigma_k^{n+1}(x), \tag{8a}$$

$$\sigma_k^{n+1}(x) = H_{0k} \left[\varepsilon^{n+1}(x) + b_k \varepsilon^n(x) \right] - a_k \sigma_k^n(x), \tag{8b}$$

whose corresponding transfer function is given by:

$$H(z) = \frac{\sigma(z)}{\varepsilon(z)} = \sum_{k=1}^{N_f} H_{0k} \frac{1 + b_k z^{-1}}{1 + a_k z^{-1}}. \tag{9}$$

The procedure to obtain the filter parameters from experimental data will be explained in Section 4.A.

C. Discretization schemes

In order to solve Equations (4), we now propose a finite difference (FD) scheme, choosing the same time step Δt as the one associated to the digital filter and discretizing the interval $[0, L]$ with N_x points, with $x_j = j\Delta x$ and $\Delta x = L/N_x$. We introduce a staggered grid and define u_j^n and f_j^n on the nodes defined by $x_j, \ 0 \leq j \leq N_x$, and $\sigma_{j+1/2}^n$ on the nodes defined by $x_{j+1/2} = x_j + \Delta x/2, \ 0 \leq j \leq N_x - 1$. Considering a leap frog scheme in time and second-order centered schemes in space, the equations of the FD scheme are:

$$\sigma_{j+1/2}^{n+1} = \sum_{k=1}^{N_f} \sigma_{k,j+1/2}^{n+1}, \tag{10a}$$

$$\sigma_{k,j+1/2}^{n+1} = \sum_{k=1}^{N_f} H_{0k} \left[\frac{u_{j+1}^{n+1} - u_j^{n+1}}{\Delta x} + b_k \frac{u_{j+1}^n - u_j^n}{\Delta x} \right] - a_k \sigma_{k,j+1/2}^n, \tag{10b}$$

$$\rho \frac{u_j^{n+1} - 2u_j^n + u_j^{n-1}}{\Delta t^2} = \frac{\sigma_{j+1/2}^n - \sigma_{j-1/2}^n}{\Delta x} + f_j^n. \tag{10c}$$

Let us note that this scheme is explicit and second order accurate in space and time.

Following the work of Bécache *et al.* [5], we perform a stability analysis of the FD scheme using energetic methods, which yields the following conditions on the filter parameters:

$$|a_k| \leq 1, \qquad |b_k| \leq 1, \qquad a_k \geq b_k, \qquad 0 \leq k \leq N_f, \tag{11}$$

and on the simulation parameters Δx and Δt (or F_s):

$$\Delta t \leq \Delta t_{\text{lim}} = h\sqrt{\rho} \left[\sum_{k=1}^{N_f} H_{0k} \frac{1 - b_k}{1 - a_k} \right]^{-1/2} \qquad \text{or} \qquad F_s \geq F_{s,\text{lim}} = \frac{1}{h\sqrt{\rho}} \left[\sum_{k=1}^{N_f} H_{0k} \frac{1 - b_k}{1 - a_k} \right]^{1/2}. \tag{12}$$

The conditions on the filter parameters mean that causality and stability are ensured ($|a_k| \leq 1$), that it is a minimum phase filter ($|b_k| \leq 1$) and that the filter response corresponds to a dissipative damping model ($a_k \geq b_k$) [4]. The condition (12) is a classical CFL condition. As explained by Bilbao [6], it is desirable to choose the sampling rate F_s close to $F_{s,\text{lim}}$ in order to minimize numerical dispersion and dissipation due to FD schemes.

4 APPLICATION TO THE LONGITUDINAL VIBRATIONS OF A NYLON CANTILEVER BEAM

We present in this final Section a numerical example where the digital filter introduced in Section 3 is designed using the measurements of Section 2.

A. Digital filter design

The parameters H_{0k}, a_k and b_k of the N_f first order filters considered in Equation (8) are found from experimental data by minimizing the following cost function in the frequency domain:

$$\mathscr{L}\left(\{a_k, b_k, H_{0k}\}_{k=1..N_f}\right) = \sum_{k=1}^{N_p} \left(\frac{\text{Re}[E_c(\omega_k)] - \text{Re}[H(e^{i\omega_k \Delta t})]}{\text{Re}[E_c(\omega_k)]} \right)^2 + \left(\frac{\text{Im}[E_c(\omega_k)] - \text{Im}[H(e^{i\omega_k \Delta t})]}{\text{Im}[E_c(\omega_k)]} \right)^2, \quad (13)$$

where $E_c(\omega_k) = E(\omega_k)(1 + i\eta(\omega_k))$ is the complex Young modulus at a set of N_p angular frequencies ω_k, $\eta(\omega_k)$ is the corresponding loss factor and $H(e^{i\omega_k \Delta t})$ is the filter response given by Equation (9) at frequency ω_k. The nonlinear optimization problem to be solved is then:

$$\min_{\{a_k, b_k, H_{0k}\}} \mathscr{L}\left(\{a_k, b_k, H_{0k}\}_{k=1..N_f}\right), \quad (14)$$

under the constraints:

$$|a_k| \leq 1, \qquad |b_k| \leq 1, \qquad a_k \geq b_k, \qquad 0 \leq k \leq N_f. \quad (15)$$

This problem is solved using the interior-point algorithm implemented in the *fmincon* MATLAB function.

Table 2: Filter parameters considering N_f first-order filters in parallel with a sampling rate $F_s = 86$ kHz.

N_f	H_{0i}	a_i	b_i	$F_{s,lim}$ (kHz)	err(Re) (%)	err(Im) %
1	3.20×10^9	-0.7931	-0.8047	83.71	3.6	45.0
2	1.60×10^9	-0.9888	-0.9905	83.88	3.9	19.1
	1.60×10^9	-0.6316	-0.6643			
3	1.07×10^9	-0.8031	-0.8215	85.20	4.8	14.2
	1.07×10^9	-0.9913	-0.9933			
	1.07×10^9	0.1730	-0.0766			

To identify the filter parameters corresponding to the experimental data presented in Section 2, the real part E of E_c is set at 3.2×10^9 GPa and its imaginary part is given by $E\,\eta(\omega_k)$ for the $N_p = 40$ data points of Figure 3, with $\eta(\omega_k) = 2\alpha/\omega_k$. The optimization procedure is performed considering 1, 2 or 3 filters in parallel. The filter parameters are given in Table 2 and the associated frequency-dependent loss factor is plotted in Figure 4. To assess the quality of the optimization, we define the following errors on the real and imaginary parts of the difference between filter output and experimental data:

$$\text{err(X)} = \left[\frac{\sum_{k=1}^{N_p} \left(\text{X}[E_c(\omega_k)] - \text{X}[H(e^{i\omega_k \Delta t})] \right)^2}{\sum_{k=1}^{N_p} \left(\text{X}[E_c(\omega_k)] \right)^2} \right]^{1/2}, \quad (16)$$

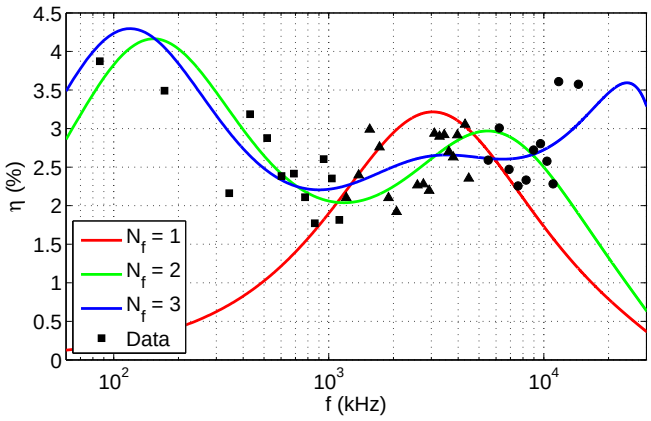

Figure 4: Frequency-dependent loss factor corresponding to the association of N_f filters in parallel.

with X stands for Re or Im. Table 2 shows that err(Im) decreases quickly from 45% to 14% when N_f increases from 1 to 3, while err(Re) remains below 5%. It is also clear in Figure 3 that the use of 3 filters in parallel allows us to better follow the experimental frequency fluctuations. We noticed that increasing further the number of filters ($N_f \geq 4$) does not improve the fit, which can be explained by the inherent frequency fluctuations in the experimental data. Finally we can check that $F_{s,lim}$ remains below the chosen sampling rate of 86 kHz, which will guarantee the stability of the numerical simulations presented hereafter.

B. Beam vibration simulations

We consider a nylon beam of length $L = 1\,\text{m}$, cross-section $S = 4\,\text{cm}^2$ and of density $\rho = 1149\,\text{kg.m}^{-3}$. This beam is excited at the right end by an impact of duration $t_{\text{imp}} = 0.3\,\text{ms}$ and of maximum intensity $F_{\text{imp}} = 1\,\text{kN}$, modeled by:

$$f(x,t) = \begin{cases} -\frac{F_{\text{imp}}}{2S}\left[1+\cos\left(\frac{\pi(2t-t_{\text{imp}})}{t_{\text{imp}}}\right)\right]\delta(x-L) & t < t_{\text{imp}}; \\ 0 & t \geq t_{\text{imp}}. \end{cases} \tag{17}$$

To obtain a good accuracy of the simulation, a minimum of 10 points per wavelength is required. Choosing a spatial step $\Delta x = 2\,\text{cm}$, the minimum wavelength that the calculation can represent is $\lambda_{min} = 20\,\text{cm}$. For a Young modulus of $E = 3.2\,\text{GPa}$ for nylon, or a longitudinal phase velocity $c = \sqrt{E/\rho} = 1669\,\text{m/s}$, the maximum frequency of the calculation is thus $f_{max} = c/\lambda_{min} = 8.3\,\text{kHz}$.

We now present the results of the time-domain simulations using the filter parameters of Table 2 and the excitation of Equation (17). The simulations are performed over a duration of 1 s and the beam displacement at $x = L/2$ is plotted in Figure 5(a) over the first 30 ms. The difference between the three simulations is seen very rapidly. The corresponding power spectral densities displayed in Figure 5(b) are calculated over a 1 s duration using a frequency resolution of 1 Hz. The theoretical frequencies for the first 12 modes of the cantilever beam calculated with $E = 3.2 \times 10^9\,\text{GPa}$ are also plotted as references. At the first mode frequency of 417 Hz, the simulation with 1 filter has an amplitude 10 dB higher than the two other simulations, which can be attributed to low loss factor of the filter response at this frequency (see Figure 4). From modes 2 and 8, between 1252 Hz and 6258 Hz, the three spectra overlap relatively well, the filter responses being close over this frequency range. At higher frequencies, some discrepancies exist between the three simulations.

5 CONCLUSIONS

We have presented in this paper an experimental technique based on a time-frequency analysis of the plate impulse response and on the use of energy decay relief to estimate the damping factor over a wide frequency

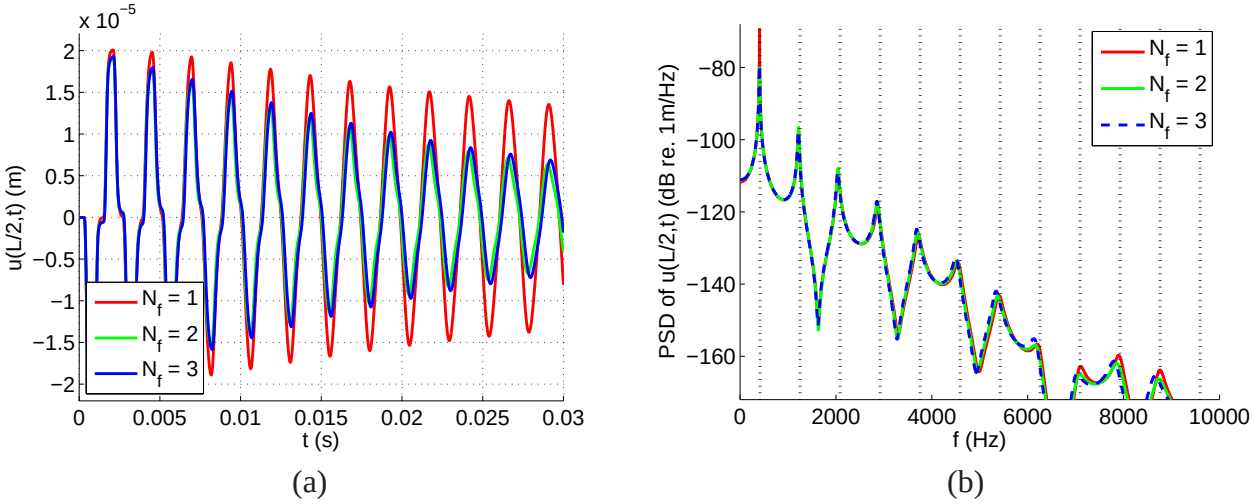

Figure 5: (a) Displacement $u(L/2,t)$ and (b) its power spectral density using 1, 2 or 3 filters. The dashed vertical lines correspond to the theoretical frequencies calculated with $E = 3.2 \times 10^9$ GPa.

range. We applied it succesfully to a nylon plate between 100 Hz and 15 kHz approximately. Then we proposed a time-domain model of an impacted structure where the material constitutive law is represented by a digital filter. The filter parameters are estimated from the experimental data through an optimization procedure that guarantees the causality and stability of the model. Time-domain simulations of the longitudinal vibrations of a nylon bar are finally presented, showing that three first-order filters in parallel are sufficient to accurately describe the frequency-dependent damping over the frequency band of interest. In the future, the optimization procedure used to obtain the filter parameters will be studied in more details, the approach will be extended to the flexural vibrations of beams and plates, and computation of acoustic quantities of interest (radiated power, directivity) will be considered.

ACKNOWLEDGEMENTS

The authors would like to thank the French “Direction Générale de l’Armement” (DGA) for supporting this work.

REFERENCES

[1] A. Farina. Simultaneous measurement of impulse response and distortion with a swept-sine technique. In *108th AES Convention, Paris, France*, 2000.

[2] K. Arcas and A. Chaigne. On the quality of plate reverberation. *Appl. Acoust.*, 71:147–156, 2010.

[3] P. Collet, G. Fary, and B. Lundberg. Noise-corrected estimation of complex modulus in accord with causality and thermodynamics: Application to an impact test. *Journal of Applied Mechanics - Transactions of the ASME*, 80(1):011018, 2013.

[4] J.O. Smith. *Introduction to Digital Filters with Audio Applications*, volume Music signal processing series. W3K Publishing, 2007.

[5] E. Bécache, A. Ezziani, and P. Joly. A mixed finite element approach for viscoelastic wave propagation. *Computational Geosciences*, 8(3):255–299, 2004.

[6] S. Bilbao. *Numerical Sound Synthesis*. Wyley, 2009.